

Performance study of the JadePix-3 telescope from a beam test

Sheng Dong^a, Zhiliang Chen^b, Jia Zhou^{c,a}, Xinye Zhai^{d,a}, Anqi Wang^c,
Yunxiang Wang^c, Hulin Wang^e, Lailin Xu^b, Jing Dong^a, Yang Zhou^a,
Yunpeng Lu^{a,*}, Mingyi Dong^{a,c}, Hongyu Zhang^{a,c}, Qun Ouyang^{a,c}

^a*State Key Laboratory of Particle Detection and Electronics, Institute of High Energy Physics, Chinese Academy of Sciences, BeiJing, 100049, BeiJing, China*

^b*University of Science and Technology of China, Hefei, 230026, Anhui, China*

^c*University of Chinese Academy of Sciences, Beijing, 100049, Beijing, China*

^d*Jilin University, Changchun, 130012, Jilin, China*

^e*PLAC, Key Laboratory of Quark & Lepton Physics (MOE), Central China Normal University, Wuhan, 430079, Hubei, China*

Abstract

We present results from a beam test of a telescope that utilizes the JadePix-3 pixel sensor, designed using TowerJazz 180 nm CMOS imaging technology. This telescope consists of 5 planes, each equipped with a JadePix-3 sensor, having pitches of $26 \times 16 \mu\text{m}^2$ and $23.11 \times 16 \mu\text{m}^2$. It also incorporates an FPGA-based synchronous readout system. The telescope underwent testing from an electron beam with energy ranging from 4 GeV to 6 GeV. At the electron energy of 5.4 GeV, the telescope provided a superior spatial resolution of 2.6 μm and 2.3 μm in two dimensions, respectively. By designating one plane as the device under test, we evaluated the JadePix-3 sensor's spatial resolution of 5.2 μm and 4.6 μm in two dimensions, and achieving a detection efficiency of more than 99.0%.

Keywords:

Beam telescope, CMOS pixel sensor, Vertex detector, Spatial resolution

*Corresponding author

Email address: yplu@ihep.ac.cn (Yunpeng Lu)

1. Introduction

The Circular Electron-Positron Collider (CEPC), proposed by the Chinese particle physics community, aims to explore the Higgs boson and provide critical tests of the underlying fundamental principles of the Standard Model, potentially unveiling new physics. As a future experimental design, it places high technical requirements on various detectors. In particular, for the vertex detector, the first layer's single-point resolution must exceed $3\text{ }\mu\text{m}$, and the power consumption of the sensors and readout electronics should remain below 50 mW/cm^2 [1, 2].

The JadePix-3 pixel sensor is a prototype design for the CEPC vertex detector which focuses on high spatial resolution with low material usage and power consumption. It involves various analog front-end circuit and digital circuit designs, the pixel matrix is segmented into four distinct sectors. There is an boundary between each sector, with a width of $20\text{ }\mu\text{m}$. Moreover, the chip contains two different pixel pitches. Figure 1 illustrates the sensor's layout, with a sensor size of $6.1 \times 10.4\text{ mm}^2$ and a pixel matrix area of $4.85 \times 8.19\text{ mm}^2$.

The functions and performance of the sensor have been tested in the laboratory. Key parameters including the minimal threshold, power consumption, noise hit rate, and position resolution have been tested, yielding preliminary results[3]. An infra-red laser beam test system is adopted to test the single-point position resolution[4], demonstrating that the resolution ranges between $pitch/2\sqrt{12}$ and $pitch/\sqrt{12}$. Given the sensor's small pitch, particularly in the row direction, it is possible to construct a high-resolution beam telescope based on this sensor. We aim to achieve two objectives: firstly, realizing a high-precision measurement tool for subsequent series of chips; and secondly, using it to test the JadePix-3 itself, and to develop a synchronized multi-layer chip readout system.

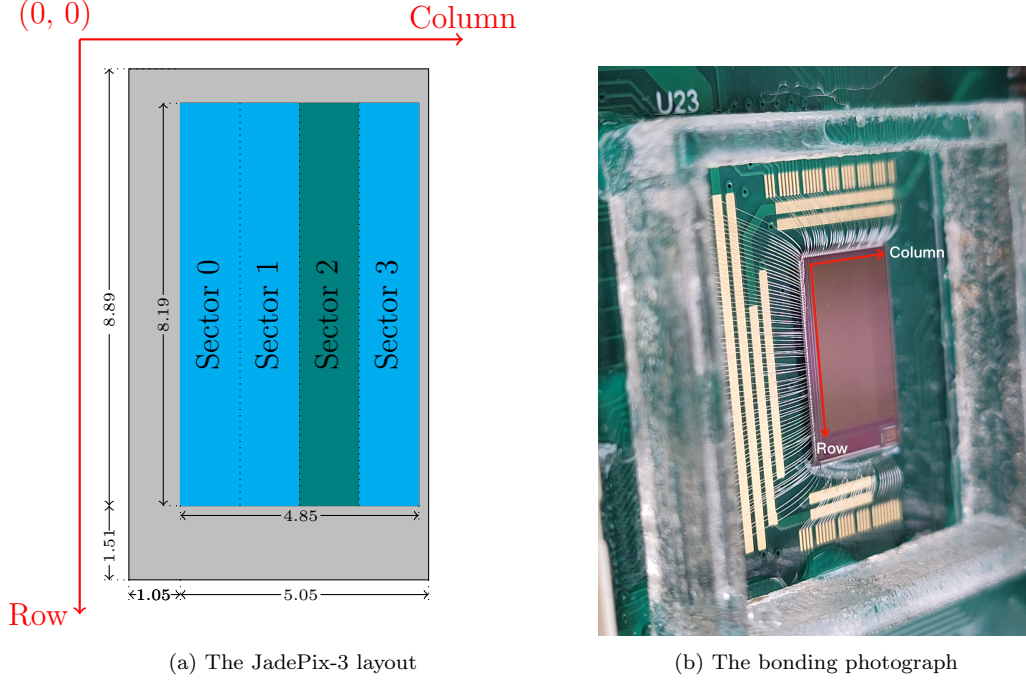


Figure 1: (a) The gray area illustrates the pixel periphery, and the cyan and teal area represents the pixel array. The pixel pitch of sector 2 is $23.11 \times 16.0 \mu\text{m}^2$, whereas sectors 0, 1, and 3 have a pitch of $26 \times 16.0 \mu\text{m}^2$. The pixel matrix of each sector consists of 48 columns and 512 rows. (b) The photograph of a bounded chip.

2. The JadePix-3 telescope implementation

2.1. Telescope setup

As shown in Figure 2, the JadePix-3 Telescope consists of 5 planes, which are P0, P1, P2, P3, P4, and P2 is the Device Under Test (DUT). The distance between the planes is 26 mm. Currently, the distance is fixed, as we have designed a magnesium-aluminum alloy metal frame to hold and protect our telescope, the frame is compact and portable, as shown in Figure 3. Single telescope plane consists of a commercial FPGA evaluation board, KC705, a sensor bonding board and an FMC adaptor which supports the communication between the sensor and the FPGA.

The global coordinate system is established as a right-handed Cartesian system, where the positive z-axis aligns with the beam direction, defining the origin within the x - y plane.

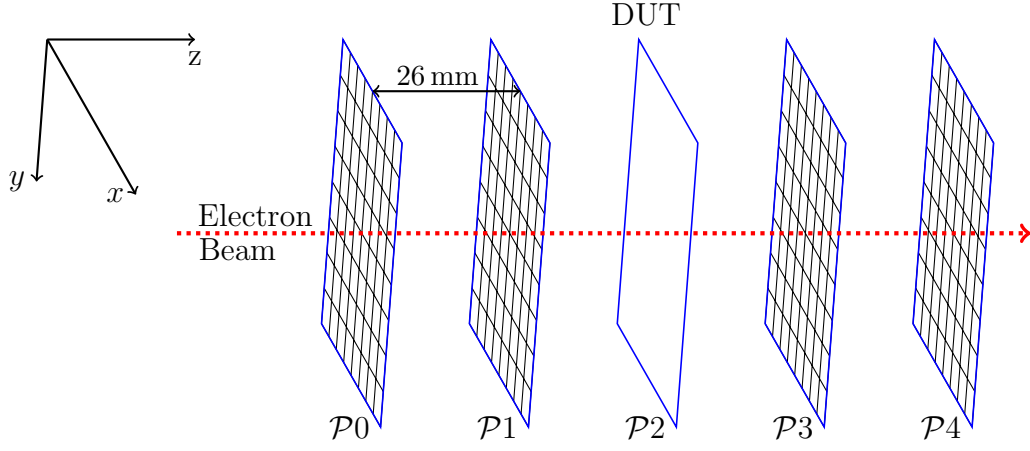


Figure 2: The JadePix-3 telescope consists of five parallel planes, with a distance of 26mm between each plane. P0, P1, P3, and P4 are reference planes, while P2 is the DUT plane.

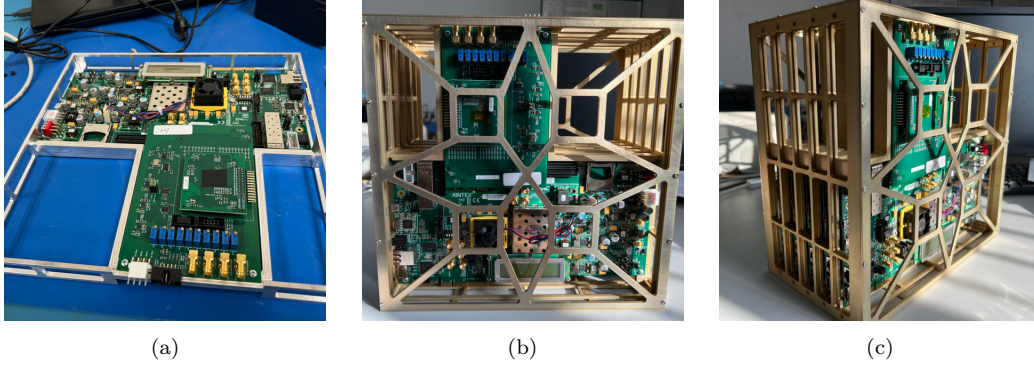


Figure 3: The photographs of the JadePix-3 telescope. (a) Single telescope plane. (b) The front view. (c) The side view.

2.2. Multi-chip synchronous readout design

A Data Acquisition (DAQ) system, based on the IPbus framework, was developed [5]. The IPbus framework, which utilizes the User Datagram Protocol (UDP) for network communication, provides excellent scalability [6]. This scalability was one of the primary reasons for choosing IPbus, as it enabled the easy expansion to a multi-chip readout system.

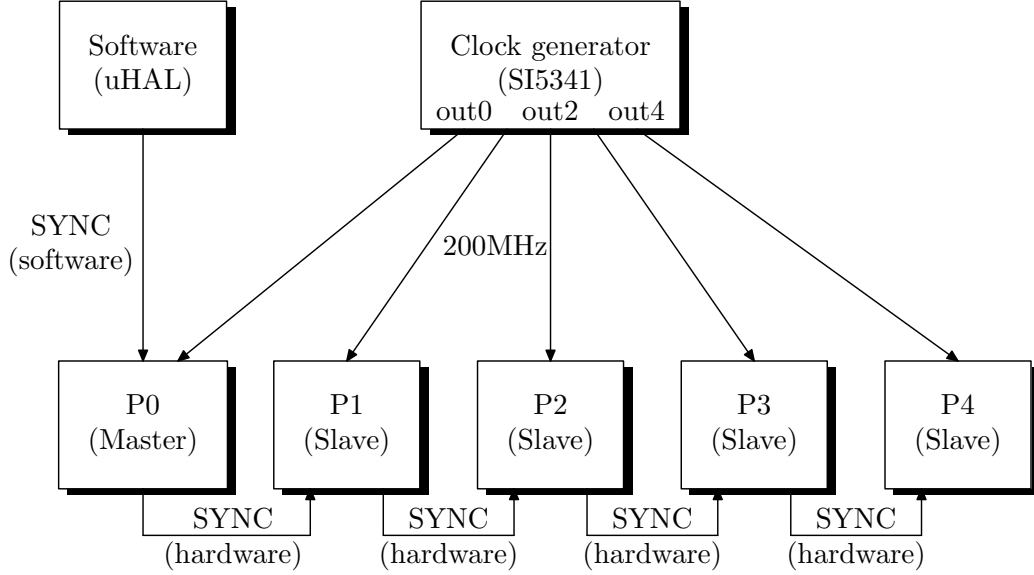


Figure 4: The telescope’s clock and synchronized readout system required software development utilizing the IPbus protocol. uHAL, functioning as the Hardware Access Library, provides an end-user API for managing IPbus transactions. Each plane in the system is loaded with identical firmware, with P0 designated as the master plane.

We utilized the SI5341-D-EVB, a commercial clock generator evaluation board, to produce 5 synchronous system clocks for each telescope plane, as shown in Figure 4. This configuration ensures the synchronization of the telescope’s operation within the same clock domain. To synchronize the start of each telescope plane, a daisy-chain signal link was designed: the synchronous start signal (SYNC) is initially generated by the software and then directed to the P0. When the master receives the SYNC (software), it generates a SYNC (hardware) signal and transmits it to the next slave plane (P1). Upon receiving the SYNC signal from the previous plane, each slave device synchronously transmits the SYNC signal to the next plane. The delay in the daisy-chain link is less than 100 ns, a duration negligible

compared to the sensor's frame integration time of $98.3\mu\text{s}$. This approach ensures that all planes begin operations almost simultaneously.

3. Experimental Set-up

The DESY-II test beam facility provides electron/positron beams with user-selectable momenta ranging from 1 GeV to 6 GeV, and a divergence of approximately 1 mrad[7]. Beam test data were collected at TB21, which is one of the three independent beam lines at the facility. The JadePix-3 telescope was positioned downstream of the beam line, behind the MIMOSA Telescope [8] and the CEPC vertex detector prototype [9]. Figure 5 shows the experimental set-up.

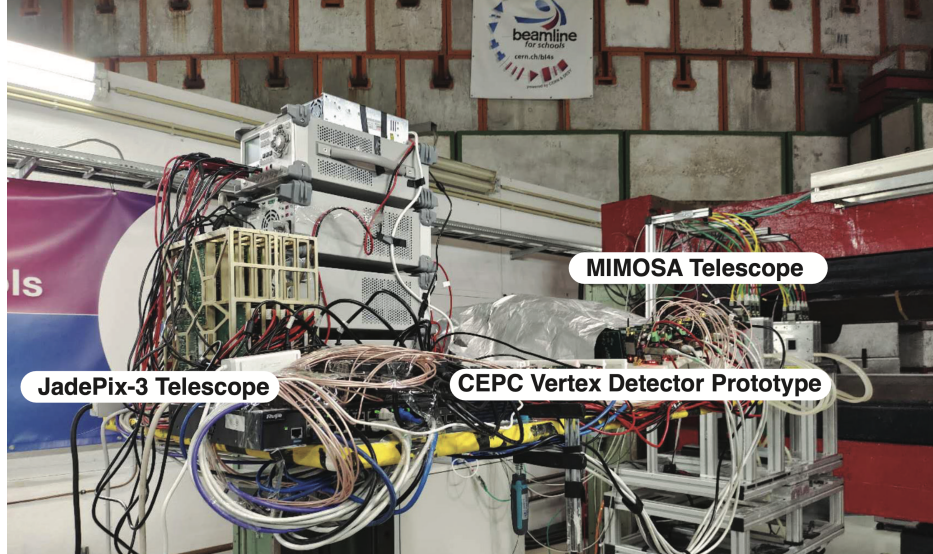


Figure 5: Experimental setup at DESY TB21: The MIMOSA Telescope was fixedly positioned upstream of the beam line. Both the JadePix-3 telescope and the CEPC vertex detector prototype shared the same movable test platform.

4. Data Analysis and Results Discussion

The Corryvreckan framework [10] is utilized for offline data analysis. An event loader module named EventLoaderJadepix3 was developed to import binary hit information from each JadePix-3 sensor's raw data file. The

Metronome module slices the data stream into regular time frames of a defined length, the time frame length is set to $98.316\text{ }\mu\text{s}$, corresponding to the rolling shutter frame readout time.

Standard modules of Corryvreckan, such as clustering, tracking, and alignment, are employed for precise alignment. Two methods for track reconstruction are employed: the straight-line and the General Broken Lines (GBL). The GBL is the primarily used reconstruction algorithm, which takes into account the effects of multiple scattering, leading to more precise analytical results. The straight-line method is utilized for analyzing track angles.

To ensure the accuracy of resolution calculations and mitigate the potential negative effects caused by the boundaries between different pitches and sectors,

For simplicity, the data from the left half (sector 0 and sector 1) were chosen for analysis, while data from the right half (sector 2 and sector 3) were excluded due to sector 2 having a different pitch. This selection implies that the pixel pitch associated with the analytical results corresponds to a size of $26 \times 16\text{ }\mu\text{m}^2$.

4.1. Cluster Size Distribution

The Clustering4D module in Corryvreckan performs clustering for detectors with timestamped hits. As JadePix-3 sensors provide binary information, the cluster position is calculated using the hits with adjacent positions and timestamps.

Figure 6a presents the cluster size (CS) distribution of DUT with a threshold set to $200\text{ }e^-$. The average cluster size is found to be 3.7, with average cluster width and height (in column and row directions) being 1.5 and 2.3, respectively, as depicted in Figure 6b. The normalized cluster size distribution, as shown in Figure 6a, shows a gradual decrease for cluster sizes greater than 2. Cluster size smaller than 4 make up 76% of the total, and those smaller than 8 constitute 93%.

Figure 7 illustrates the intra-pixel density distribution with cluster sizes of 1, 2, 3, and 4 pixels, respectively. When the CS is 1, the particle's incident position is more likely at the center of the pixel, as depicted in Figure 7a. Conversely, when the hit position is at the edge of a pixel, multiple pixels are more likely to be hit due to the charge sharing effect. Particularly, when the pixel is near the middle of the pixel boundary, two pixels hitting each other becomes more probable. This effect is especially pronounced in the x

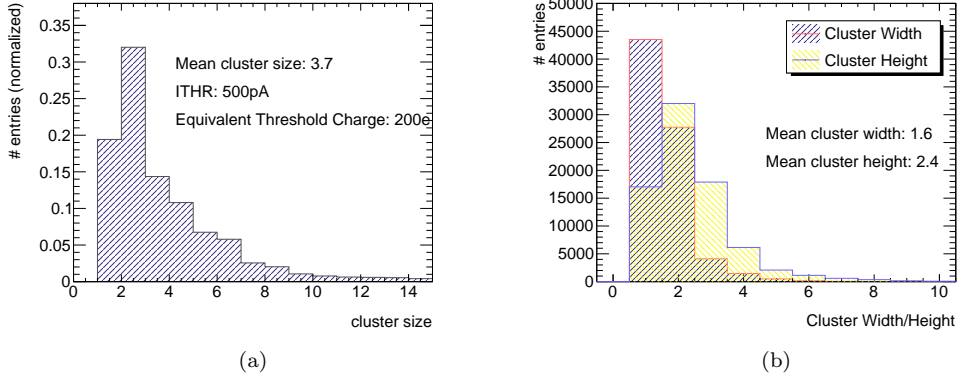


Figure 6: Experiment parameters: beam energy = 5.8 GeV, threshold = 200 e^- (a) The cluster size distribution. (b) The distribution of cluster width and cluster height.

direction, as depicted in Figure 7b. At the corners of pixels, generating hits involving four pixels is noticeably more likely, as shown in Figure 7d.

To further investigate the reasons behind the cluster distribution for a cluster size (CS) of 3, as demonstrated in Figure 7c, we concentrated on the distribution associated with various cluster patterns, as depicted in Figure 8. Two main patterns were observed: Pattern 1, as shown in Figure 8a, is characterized by three adjacent pixels firing in the the y direction. Pattern 2, demonstrated in Figure 8b, featuring two pixels fired in both the x and y directions. The occurrence rates for Pattern 1 and Pattern 2 are 53.3% and 46.3%, respectively. In Pattern 1, When the central pixel in the middle is fired, it tends to cause the pixels immediately above and below it to fire as well. For Pattern 2, firing occurs more readily at the four corners of a pixel as well as along the y directional edges, leading to adjacent pixels firing in both x and y directions.

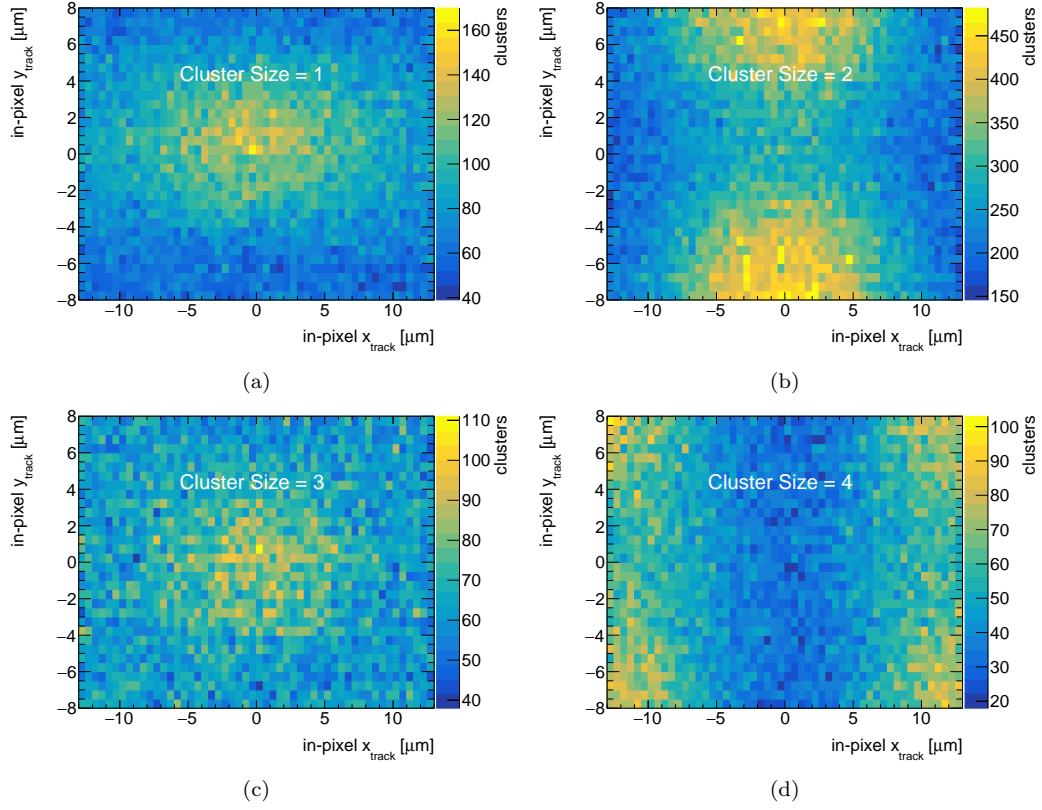


Figure 7: The unbiased intra-pixel density distribution at the DUT for cluster sizes 1 to 4, respectively.

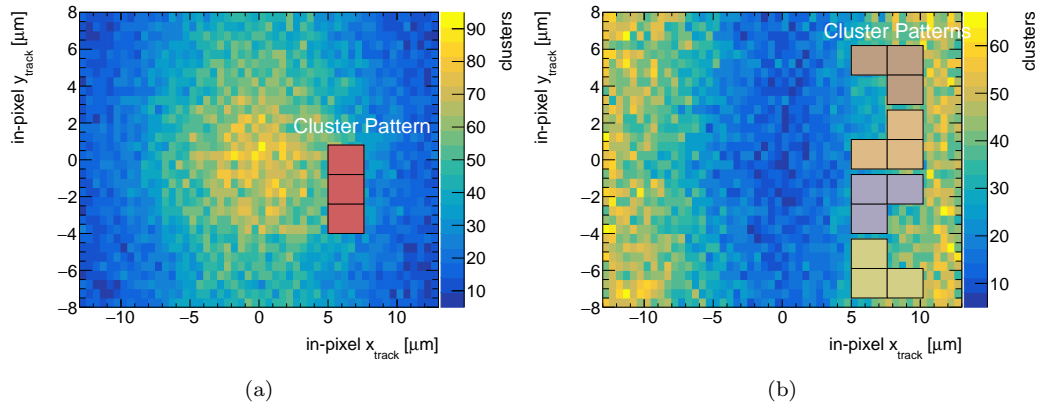


Figure 8: The intra-pixel density distribution at the DUT for CS3. (a) Cluster Pattern 1. (b) Cluster Pattern 2.

4.2. Alignment and Tracking

As suggested by the corryvreckan manual [11], the alignment procedure is as follows: 1. Pre-align the telescope planes, 2. Finely align the telescope planes, 3. Pre-align the DUT plane, 4. Finely align the DUT plane. For the telescope alignment, we stipulate that each telescope plane must concurrently have a cluster.

The alignment performance can be assessed by examining the χ^2/n_{dof} (chi-square per degree of freedom) of track fitting and the distance distribution between the track and the hit. Figure 9a presents the χ^2/n_{dof} distribution, with a mean value of 0.96. This notably low mean value suggests that the fitted tracks closely align with the cluster positions. Figure 9b illustrates the distribution of distances between the track and hit. This figure indicates that the distances in both x and y directions are minimal and, importantly, exhibit symmetry about the origin in both directions. These results collectively indicate that the tracking performance is precise and reliable.

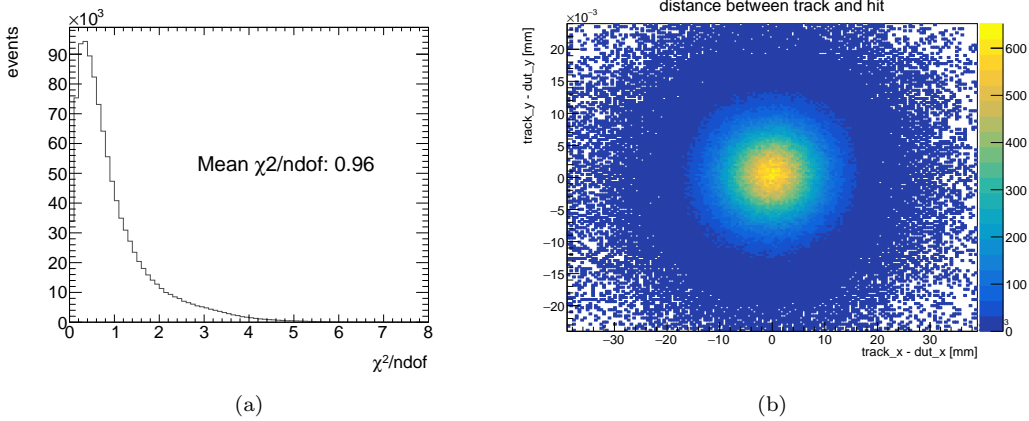


Figure 9: Experiment parameters: beam energy = 5.8 GeV, threshold = 200 e^- (a) The distribution of χ^2/n_{dof} (b) The distribution of distance between track and hit.

4.3. Residual and Spatial Resolution

Through the process of track fitting, hit prediction points corresponding to the DUT measurement points are derived. This allows for the determination of the hit residual distribution on the DUT. The unbiased residual distributions in the x and y directions are depicted in Figure 10. The red line represents the Gaussian fit of the data. The σ of the residual distribution for the DUT in the x and y directions are 6.71 μm and 5.21 μm , respectively.

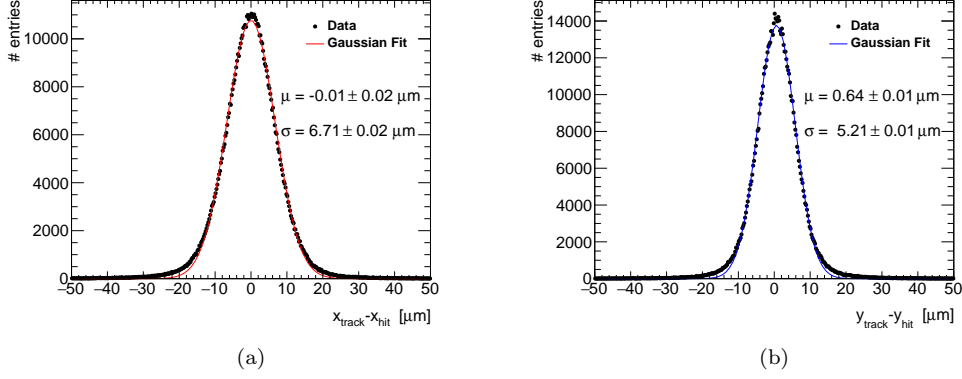


Figure 10: Experiment parameters: beam energy = 5.8 GeV, threshold = 200 e^- (a) Unbiased residual distribution in the x direction (b) Unbiased residual distribution in the y direction.

To accurately determine the spatial resolution of the DUT plane, it is essential to eliminate the contribution of the telescope system, as outlined in Equation 1. As shown in Equation 2, σ_{tel} can be related to σ_{plane} when all planes have the same intrinsic resolution, and the DUT is positioned at z_0 , with the reference planes symmetrically mounted around the DUT, a scaling factor k is defined [12]. This factor k can be calculated using Equation 3, which incorporates the distance of each plane.

$$\sigma_{meas}^2 = \sigma_{DUT}^2 + \sigma_{tel}^2 \quad (1)$$

$$\sigma_{tel}^2 = k\sigma_{plane}^2 \quad (2)$$

$$k = \frac{\sum_i^N z_i^2}{N \sum_i^N z_i^2 - (\sum_i^N z_i)^2} \quad (3)$$

By applying Equation 1 and Equation 2, we can deduce Equation 4 and Equation 5.

$$\sigma_{plane}^2 = \frac{\sigma_{meas}^2}{1 + k} \quad (4)$$

$$\sigma_{tel}^2 = \frac{k}{1 + k} \sigma_{meas}^2 \quad (5)$$

For the JadePix-3 Telescope, the scaling factor k can be calculated as 0.25. Subsequently, we can determine that the spatial resolution for the DUT are $6.0\mu\text{m}$ and $4.7\mu\text{m}$ in the x and y directions, respectively. And the resolution of the telescope are $3.0\mu\text{m}$ and $2.3\mu\text{m}$ in the x and y directions, respectively.

Figure 11 and Figure 12 illustrates the unbiased residual distributions for cluster sizes ranging from 1 to 4. For this analysis, only clusters associated with the DUT were selected. The measured spatial resolutions in the x direction, corresponding to the cluster sizes, are $9.28\mu\text{m}$, $7.19\mu\text{m}$, $5.68\mu\text{m}$ and $5.32\mu\text{m}$, respectively. The results for the y direction are $5.32\mu\text{m}$, $5.53\mu\text{m}$, $5.16\mu\text{m}$ and $4.91\mu\text{m}$, respectively, as presented in Figure 12.

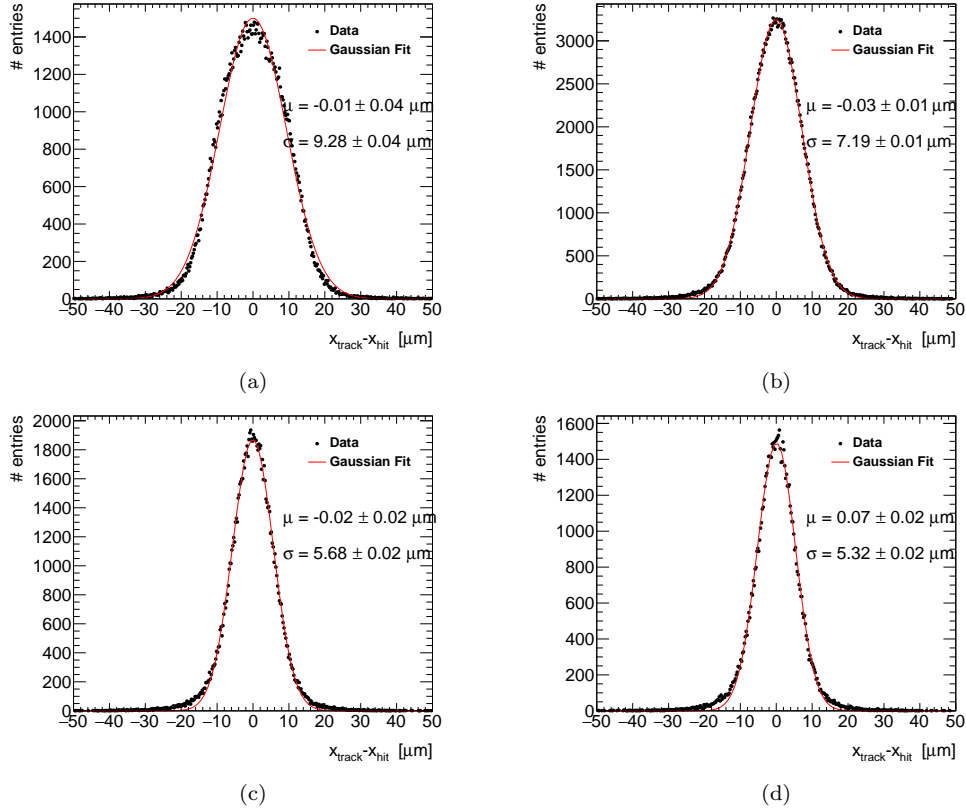


Figure 11: Distribution of residuals in the x direction for different cluster sizes. Experiment parameters: beam energy = 5.8 GeV , threshold = $200 e^-$ (a) CS = 1. (b) CS = 2. (c) CS = 3. (d) CS = 4.

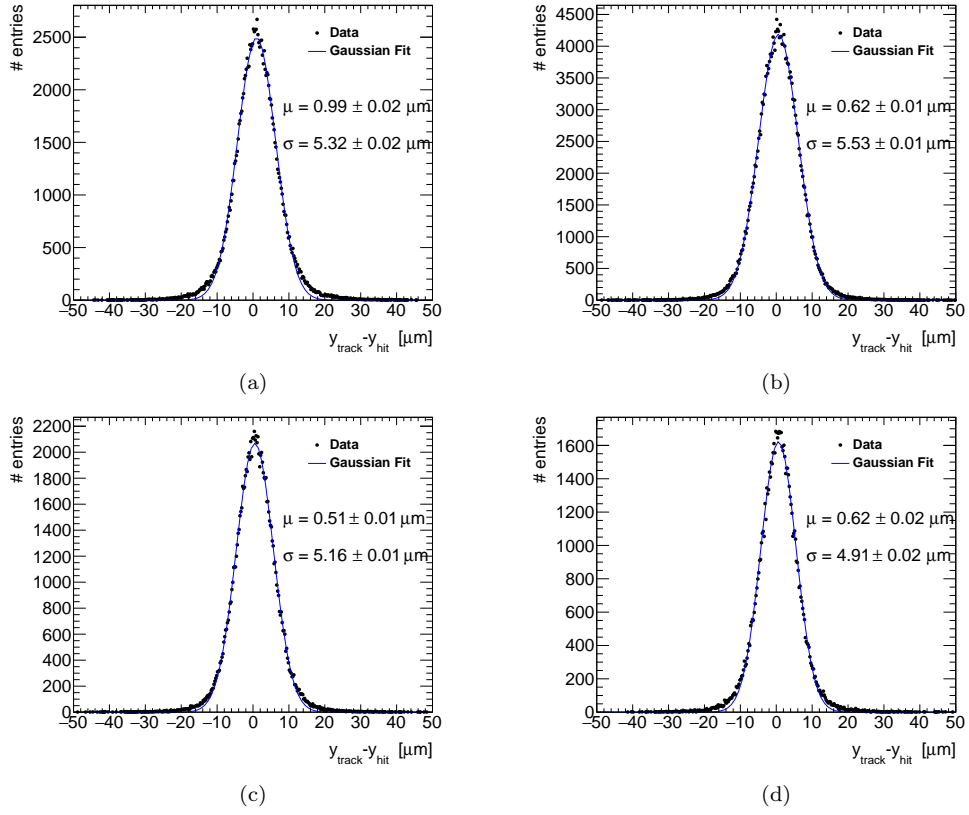


Figure 12: Distribution of residuals in the y direction for different cluster sizes. Experiment parameters: beam energy = 5.8 GeV, threshold = 200 e^- . (a) CS = 1. (b) CS = 2. (c) CS = 3. (d) CS = 4.

4.4. Efficiency

The efficiency of the DUT is defined as the fraction of tracks with associated clusters on the DUT over the total number of tracks intersecting the DUT. After all tracks have been reconstructed, subsequent data analysis discards some tracks to enhance the precision of the results. Tracks meeting the following criteria will be excluded:

- The χ^2 value exceeds a predefined limit of 10.
- Tracks located outside the Region of Interest (ROI), specifically Sector 0 and Sector 1.
- Tracks in proximity to masked pixels.
- Tracks near the edge of the rolling shutter frame.

Figure 13 presents the in-pixel efficiency map. It is observable that the likelihood of a particle being detected by the sensor increases when it strikes closer to the center of a pixel.

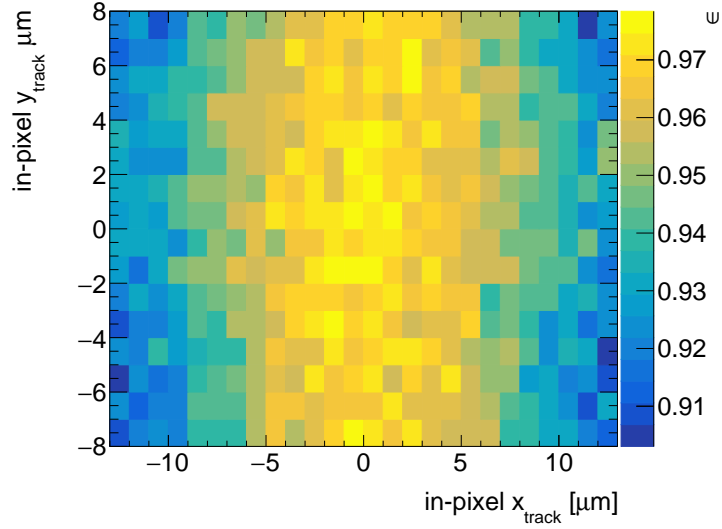


Figure 13: The efficiency map in-pixel. Experiment parameters: beam energy = 5.8 GeV, threshold = 200 e^- .

4.5. Threshold Scan

We conducted a threshold scan to assess changes in several key performance metrics of the detector under varying thresholds, including average cluster size, detection efficiency, and spatial resolution in both x and y directions. As illustrated in Figure 14a, an increase in the threshold leads to a gradual decrease in the sensor's average cluster size, accompanied by a corresponding reduction in detection efficiency, as shown in Figure 14b. These observed trends are consistent with our expectations.

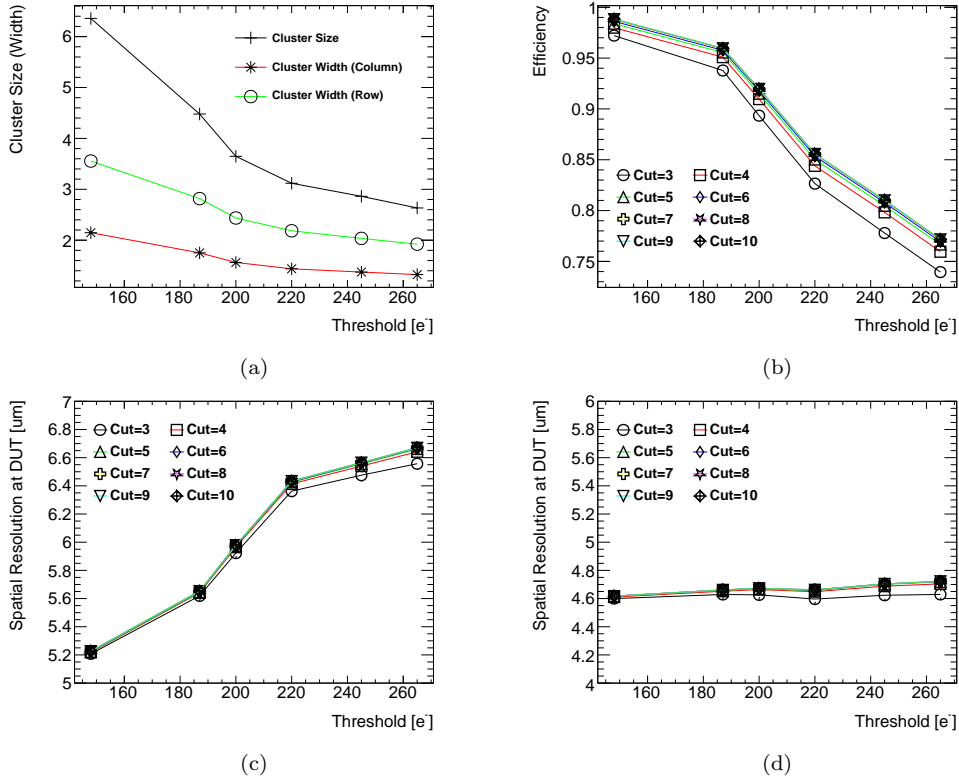


Figure 14: Experiment parameters: beam energy = 5.4 GeV, threshold range: from 148 e^- to 265 e^- (a) Mean cluster size. (b) Efficiency. (c) Residual in x direction. (d) Residual in y direction.

The figure illustrates various cuts, each indicating the level of correspondence between the reconstructed tracks and the clusters in the DUT. For example, a cut of 3 means that if a cluster in the DUT is located within a distance of three times the intrinsic resolution from the predicted hit point

on the track, this signifies a match between the track and the DUT. A larger cut signifies the aggregation of more clusters on the DUT, resulting in higher detection efficiency, as evident from Figure 14b. However, an increase in the cut size negatively affects the spatial resolution in both the x and y directions. This decrease in resolution occurs because selecting more distant clusters from the predicted hit point results in larger residuals, thus degrading the spatial resolution. Figure 14c, it is observed that within the threshold scanning range, a higher threshold reduces the spatial resolution in the x direction. While the spatial resolution in the y direction also declines, the extent of this degradation is less significant.

Based on the results of the threshold scan, to optimize the detector's performance within this threshold range, a lower threshold is preferable, as it enhances both the spatial resolution and the detection efficiency.

5. Conclusion

This work presents the development, testing, and comprehensive analysis of a beam telescope equipped with the JadePix-3 CMOS pixel sensor, including an introduction to the designs of both the sensor and the telescope. The telescope underwent extensive testing at DESY TB21 facility using an electron beam with energies ranging from 4 GeV to 6 GeV.

A thorough data analysis was conducted, including cluster size, detection efficiency, and spatial resolution. The study also included an in-depth examination of various cluster sizes, aimed at determining the differential intrinsic resolution of this telescope.

By analyzing a series of threshold scanning results, we identified the optimal operational threshold for the sensor. This enabled us to achieve the most favorable spatial resolution and efficiency for both the sensor under these specific threshold conditions.

6. Acknowledgements

This study was supported by the National Key Research and Development Program of China (Grant No. 2016YFA0400400) and the Strategic Priority Research Program of the Chinese Academy of Sciences (Grant No. XPB23).

References

- [1] C. S. Group, et al., Cepc conceptual design report: Volume 1-accelerator, arXiv preprint arXiv:1809.00285 (2018).
- [2] C. S. Group, et al., Cepc conceptual design report: Volume 2-physics & detector, arXiv preprint arXiv:1811.10545 (2018).
- [3] S. Dong, P. Yang, Y. Zhang, Y. Zhou, H. Wang, L. Xiao, L. Zhang, Z. Shi, D. Guo, Z. Wu, et al., Design and characterisation of the jadepix-3 cmos pixel sensor, Nuclear Instruments and Methods in Physics Research Section A: Accelerators, Spectrometers, Detectors and Associated Equipment 1048 (2023) 167967.
- [4] Y. Liu, Y. Lu, X. Ju, O.-Y. Qun, Test of a fine pitch soi pixel detector with laser beam, Chinese Physics C 40 (1) (2016) 016202.
- [5] S. Dong, Y. Lu, H. Wang, G. Huang, W. Dong, The daq and control system for jadepix3, Journal of Instrumentation 16 (07) (2021) P07052.
- [6] C. G. Larrea, K. Harder, D. Newbold, D. Sankey, A. Rose, A. Thea, T. Williams, Ipbu: a flexible ethernet-based control system for xtca hardware, Journal of instrumentation 10 (02) (2015) C02019.
- [7] R. Diener, J. Dreyling-Eschweiler, H. Ehrlichmann, I.-M. Gregor, U. Kötzt, U. Krämer, N. Meyners, N. Potylitsina-Kube, A. Schütz, P. Schütze, et al., The desy ii test beam facility, Nuclear Instruments and Methods in Physics Research Section A: Accelerators, Spectrometers, Detectors and Associated Equipment 922 (2019) 265–286.
- [8] J. Baudot, G. Bertolone, A. Brogna, G. Claus, C. Colledani, Y. Degerli, R. De Masi, A. Dorokhov, G. Doziere, W. Dulinski, et al., First test results of mimosa-26, a fast cmos sensor with integrated zero suppression and digitized output, in: 2009 IEEE Nuclear Science Symposium Conference Record (NSS/MIC), IEEE, 2009, pp. 1169–1173.
- [9] T. Wu, S. Li, W. Wang, J. Zhou, Z. Yan, Y. Hu, X. Zhang, Z. Liang, W. Wei, Y. Zhang, et al., Beam test of a 180 nm cmos pixel sensor for the cepc vertex detector, Nuclear Instruments and Methods in Physics Research Section A: Accelerators, Spectrometers, Detectors and Associated Equipment 1059 (2024) 168945.

- [10] D. Dannheim, K. Dort, L. Huth, D. Hynds, I. Kremastiotis, J. Kröger, M. Munker, F. Pitters, P. Schütze, S. Spannagel, et al., Corryvreckan: a modular 4d track reconstruction and analysis software for test beam data, *Journal of Instrumentation* 16 (03) (2021) P03008.
- [11] J. Kröger, S. Spannagel, M. Williams, User manual for the corryvreckan test beam data reconstruction framework, version 1.0, arXiv preprint arXiv:1912.00856 (2019).
- [12] A. Bulgheroni, E.-J. Consortium, et al., Results from the eudet telescope with high resolution planes, *Nuclear Instruments and Methods in Physics Research Section A: Accelerators, Spectrometers, Detectors and Associated Equipment* 623 (1) (2010) 399–401.